Phase Crossover induced by Dynamical Many Body Localization in Periodically Driven Long-Range Spin Systems

Mahbub Rahaman,[1] Takashi Mori,[2] and Analabha Roy[1]

[1] *Department of Physics, The University of Burdwan, Golapbag, Bardhaman - 713 104, India*
[2] *RIKEN CEMS, 2-1 Hirosawa, Wako, Saitama, 351-0198, Japan*

Dynamical many-body freezing occurs in periodic transverse field-driven integrable quantum spin systems. Under resonance conditions, quantum dynamics causes practically infinite hysteresis in the drive response, maintaining its starting value. We extended this to non-integrable many body systems by reducing the Hamiltonian symmetries through a power-law dependence in spin exchange energy, $J_{ij} = 1/|i-j|^{\beta}$. The dynamics of the integrable short-range Transverse Field Ising Model (TFIM) and non-integrable long-range Lipkin Meshkov-Glick (LMG) models were investigated. In the LMG, the resonance conditions in the driving field suppresses the heating postulated by the *Eigenstate Thermalization Hypothesis* (ETH) by inducing *Dynamical Many Body Localization*, or DMBL. This is in contrast to Many Body Localization (MBL), which requires disorder to suppress ETH. DMBL has been validated by the Inverse Participation Ratio (IPR) of the quasi-stationary Floquet modes. While TFIM has IPR localization for all drive parameters, the LMG exhibits high-frequency localization only at the resonances. IPR localization in the LMG deteriorates with an inverse system size law at lower frequencies, which indicates heating to infinite temperature. Furthermore, adiabatically increasing frequency and amplitude from low values raises the Floquet state IPR in the LMG from nearly zero to unity, indicating a phase crossover. This occurrence enables a future technique to construct an MBL engine in clean systems that can be cycled by adjusting drive parameters only.

Keywords: Dynamical localization, Thermalization, Phase Crossover

Periodically driven Quantum Many Body Systems can experience Dynamical Freezing (DMF) when dynamical hysteresis stops observables from reaching their diagonal averaged values and thermalizing to infinite temperature [1–3]. Under certain resonance conditions in the drive parameters, DMF can cause the response to 'freeze' completely to its initial value at all times. This arises as a consequence of additional approximate symmetries that occur at resonance. DMF has been demonstrated via the Rotating Wave Approximation (RWA) in the driven TFIM with nearest neighbour interactions [4] and is shown to be protected when translational invariance is explicitly broken (say, by disorder) [5, 6].

The utilization of Floquet theory simplifies the analysis of time-periodic systems. For closed quantum systems governed by the time-dependent Schrödinger equation, the *Floquet Hamiltonian* allows for a mapping of the time-dependent dynamics into the dynamics of a time-independent effective Hamiltonian, provided the system is strobed at integer multiples of the time period of the drive. The time independent eigenstates of the effective Hamiltonian correspond to quasi-stationary *Floquet Modes* of the original Hamiltonian. The temporal progression of the system comes from phase coefficients that capture the dynamics [7, 8].

Any sufficiently complex non-integrable Many Body System is expected to thermalize according to the Eigenstate Thermalization Hypothesis (ETH) despite the fact that closed quantum dynamics preserves the memory of the initial state of the system. This arises due to the properties of the matrix elements of observables in typical states[9]. The ETH can be readily adapted to time-periodic systems using Floquet theory (the Floquet-ETH, or FETH). Nonetheless, the conditions for ETH to hold are not particularly strong, and the density matrix of the system can fail to approach one that is described by a thermal expression. In such cases, the system is said to undergo *Many Body Localization* (MBL)[10]. This phenomenon is stable against local perturbations, and constitutes an exotic state of matter with far-reaching implications in theoretical physics, as well as in practical applications[11].

The addition of disorder has been identified as a crucial component in the onset of MBL. In that case, thermalization is prevented by disorder-induced localization. Nonetheless, alternative approaches to MBL in disorder-free systems can be acheived by time-periodic driving. For instance, MBL has been detected in systems like periodically driven spinless fermions at nearest neighbour hopping [12] or engineered by employing heavy particles to generate dynamically an effective disorder [13] or in a periodically driven disorder-free hard core many body superfluid bosons, drop in current and saturation at work done ascertains localization[14]. An alternative approach to realizing MBL in disorder-free many-body system involves *Floquet Engineering*, where a time-periodic drive is introduced, and the drive parameters tuned so as to

Need to check refs 20-31, as well as

introduce a clustering of quasistationary energies in a manner similar to localization[9].

In this article, we propose that additional approximate symmetries can be Floquet-engineered in quantum many body systems with lower symmetry than the TFIM, such as those with long-range interactions. This results in both DMF and MBL occurring simultaneously at resonant values of the drive parameters, and complete thermal behaviour at other values. This phenomenon is distinct from DMF in the TFIM, since clean TFIM systems, being integrable, never thermalize.

To demonstrate the onset of MBL, we investigate the driven Lipkin-Meshkov-Glick (LMG) model, a long-range system that is a special case of the more general Curie-Weiss model, wherein the nearest-neighbour exchange in the TFIM is extended to longer ranges with a power law dependence, $J_{ij} \sim 1/|i-j|^{\beta}$ [15–17]. Setting $\beta=\infty$ recovers the TFIM, and setting $\beta=0$ yields the LMG model. We have recovered the onset of DMF in this system and have supported our result with numerical simulations.

In addition, we compare the degree of localization of the quasi-stationary Floquet modes in both limits of β. In order to do so, we look at the Inverse Participation Ratio (IPR) of the Floquet modes in the representation given by the eigenstates of the symmetry-breaking field. The IPR, closely related to the concept of quantum purity, is defined as the formal sum of the square of the density in some physically meaningful space or representation. A high IPR of a stationary state denotes low participation in most of the representation, and a low IPR distributes participation uniformly across the representation, leading to ergodic dynamics[18]. Thus, IPR [19] is a useful tool for witnessing MBL of a quantum system. For an MBL system, the IPR is unity, and it scales inversely with the system size when it is thermally distributed [20].

In the first section of this paper, we present all essential theoretical frameworks. Our results for the LMG model are presented next in section II. In that section, we have used the Rotating Wave Approximation (RWA) [21], where only the slowest rotating terms in the Fourier expansion of the Hamiltonian in a frame co-rotating with the symmetry breaking drive field are retained. In addition, we have the obtained analytical expressions for the Floquet modes and their IPR. They are used to probe the system dynamics in the high and low-frequency domains at both limits of β. In section III we have used phase space plots to contrast the low and high frequency limits of the LMG model in the thermodynamic limit by mapping it to an equivalent classical Hamiltonian system. Finally, in section IV, we have looked at numerical computations of the IPR of the Floquet modes for different values of the drive parameters, well beyond those that allow for the RWA. We observed that, if the system is driven by an adiabatically increasing drive frequency from low to high limit while remaining in the resonance region, a sharp crossover from a thermal to an MBL phase occurs. We conclude with discussions and outlook.

I. BACKGROUND

The Eigenstate Thermalization Hypothesis (ETH) is a series of conjectures that allows for the thermalization of an isolated quantum many body system. The state of the system, $|\psi(t)\rangle$, evolves according to the Schrödinger equation $\hat{H}\,|\psi(t)\rangle = i\dfrac{\partial}{\partial t}\,|\psi\rangle$. The Hamiltonian $\hat{H}$ is assumed to be *non-integrable*, in that it lacks an extensive number of *local* additive conserved quantities, that is to say, there are no set of observables $\hat{O}_s$ such that $\hat{H} = \sum_s \hat{O}_s$ for any extensive index s. Here, the $\hat{O}_s$ constitute an arbitrary CSCO (complete set of commuting observables) that are *local*, having sub-extensive support in the system size. In addition, we postulate the existence of an equivalent Hamiltonian $\hat{H}_{eq}$ for every Hamiltonian $\hat{H}$ as well as an "equilibrium" value A_{eq} for every observable $\hat{A}$, such that

$$A_{eq}(E) \equiv \frac{\mathrm{Tr}\left(\hat{A}e^{-\beta\hat{H}_{eq}}\right)}{\mathrm{Tr}\left(e^{-\beta\hat{H}_{eq}}\right)}. \tag{1}$$

where $E = \langle\psi(t)|\hat{H}|\psi(t)\rangle$ is the conserved energy of the system, and $\beta = 1/(k_B T)$ is the inverse temperature, H_{eq} is an effective Hamiltonian that captures the long-time average dynamics of the system, and k_B is the Boltzmann constant.

To put it simply, ETH proposes that this many-body Hamiltonian undergoes thermalization as seen in the *long-time averages* of observables, with the eigenstates bearing resemblance to thermal states. The aforementioned hypothesis serves as a valuable instrument for comprehending the conduct of stimulated quantum systems and their correlation with thermal equilibrium. This assertion can be justified by examining the expectation value of an observable $\hat{A}$ as it evolves under the Schrödinger equation. To see this, we first expand the state of the system $|\psi(t)\rangle$ as:

$$|\psi(t)\rangle = \sum_m c_m(t)\,|m(0)\rangle\,,$$

where $|m(0)\rangle$ represents the eigenstates of $\hat{H}(0)$ with energy E_m. The coefficients $c_m(t)$ describe the time-dependent amplitude of the expansion. Plugging these expansions into the expression for the expectation value, we obtain the long-time average of the expectation value [22]:

$$\overline{\left\langle \hat{A}(t) \right\rangle} = \sum_{m,k} \overline{c_m^*(t) c_k(t)} \left\langle m(0)|\hat{A}|k(0)\right\rangle , \tag{2}$$

where the overline indicates the following operation for any time-dependent quantity $\mathcal{O}(t)$,

$$\overline{\mathcal{O}} \equiv \lim_{t\to\infty} \frac{1}{t} \int_0^t \mathrm{d}\tau \; \mathcal{O}(\tau). \tag{3}$$

Had the system been integrable, the large number of conserved quantities would restrict mixing between the states during unitary evolution. In the non-integrable case, the system explores the entire Hilbert space spanned by eigenstates with eigenvalues close to E more-or-less uniformly. In that case, the matrix elements $\langle m(0)|\hat{A}|k(0)\rangle$ are said to satisfy the Srednicki ansatz [23, 24]:

$$\begin{aligned}\langle m(0)|\hat{A}|k(0)\rangle &\approx A_{eq}\left(\frac{E_m + E_k}{2}\right)\delta_{mk} + \\ & e^{-\frac{1}{2}S\left(\frac{E_m+E_k}{2}\right)} f\;\left(\frac{E_m + E_k}{2}, E_m - E_k\right) R_{mk}. \end{aligned} \tag{4}$$

Here, S is the thermodynamic entropy and R_{mk} are elements of a random matrix with vanishing mean and unit variance. What this means for the ensuing dynamics is that the system explores the accessible Hilbert space uniformly, and the matrix elements $\langle m(0)|\,\hat{A}(t)\,|k(0)\rangle$ become indistinguishable for most pairs of m and k. Applying this ansatz and taking the thermodynamic limit by ignoring terms $\mathcal{O}(e^{-S/2})$, the expression for the expectation value becomes:

$$\begin{aligned}\overline{\left\langle \hat{A}(t) \right\rangle} &\approx \sum_m \overline{\left|c_m(t)\right|^2}\; A_{eq}\left(\frac{E_m + E_k}{2}\right) \\ &\approx A_{eq}(E) \sum_m \overline{\left|c_m(t)\right|^2} = A_{eq}(E),\end{aligned}$$

where, in the last step, we utilized the fact that A_{eq} is a smooth function, and that the states with energies far from E have $\left|c_m(t)\right|^2 \approx 0$. Therefore, in the limit of large systems the expectation value of an observable $\hat{A}$ is approximately equal to the thermal expectation value A_{eq}. This is the essence of the ETH, which suggests that individual eigenstates of a quantum system can be described by statistical mechanics in the long-time limit.

We now generalize the ETH to non-integrable many body systems that are closed, but not isolated. In that case, it is possible to impart a periodic time-dependence on the Hamiltonian while still ensuring unitary evolution. If the time period of the drive is T, and the corresponding drive frequency $\omega \equiv 2\pi/T$, the Floquet theorem states that the solutions to the Schrödinger equation can be written as $|\psi(t)\rangle = e^{-i\epsilon t/\hbar}\,|\phi(t)\rangle$, where the $|\phi(t)\rangle$ are T-periodic states called *Floquet Modes*, the corresponding $\epsilon \in \mathbb{R}$, are called *quasienergies*. Quasienergy values are not unique, and can be made to be bounded within a Floquet photon,*viz.* a range $[-\omega/2, \omega/2]$[25, 26]. As a consequence, the unitary evolution operator can be spit into two parts as follows [27].

$$U(t) = e^{-i\hat{K}_F(t)}\, e^{-i\hat{H}_F t}. \tag{5}$$

Here, the micromotion operator $\hat{K}_F(t)$ is time-periodic in T, with $\hat{K}_F(0) = 0$, and the Floquet Hamiltonian $\hat{H}_F = \hat{H}(t) - i\left.\frac{\partial}{\partial t}\right|_{t=T}$. Thus, if the system is strobed at integer multiples of T only, then the unitary evolution matches that of a time independent Hamiltonian H_F. This can capture most of the exact dynamics at large frequencies.

In such systems, the Floquet Eigenstate Thermalization Hypothesis (FETH) posits that, subject to specific conditions and in the context of a system of significant size, the Floquet modes themselves exhibit thermal state-like behavior, *i.e.*, $\hat{H}_{eq} \approx \hat{H}_F$ in eqn 1. However, in contrast to the isolated systems, the loss of energy conservation allows for the mixing of all Floquet modes in the ensuing dynamics, not just those with quasienergies near E. Were this to actually happen in the ensuing dynamics, it can be reconciled with ETH [28] by ensuring that $\beta = 0$ in eq 1. In other words, the nonequilibrium steady state of the system tends to an infinite temperature, maximum entropy density matrix.

However, drive parameters like amplitude, frequency, and duty-cycle strongly affect the structure of the Floquet modes $|\phi\rangle$. Thus, they can be engineered to prevent the kind of full mixing that would lead to infinite temperatures, manifesting suppression of thermalization dynamically. Thus, this type of *Floquet Engineering* can produce *Dynamical Many Body Localization* (DMBL), where the system fails to reach thermal equilibrium and remains localised, possibly near its initial state, even at large times. This paradigm seems similar to standard Many-Body Localization[29, 30], where disorder, locality, and integrability can cause athermality via breakdown in the Srednicki ansatz. However, DMBL is a purely dynamical phenomenon, and thus can occur regardless of disorder, locality of observables, or system integrability, all of which have been studied for MBL onset [31–33].

Integrable Many Body systems do not exhibit thermalization. When subjected to time-periodic drives, Floquet engineering allows for the introduction of additional approximate conserved quantities that dynamically suppress the evolution of certain observables by hysteresis. This type of *freezing* of response has been shown in integrable systems [6]. A paradigmatic example is the driven Transverse Field Ising model (TFIM) in one dimension [34]. The Hamiltonian is given by

$$\hat{H}(t) = \hat{H}_0 + h_z(t)\ \hat{H}_1 \tag{6}$$

$$\hat{H}_0 = -\frac{1}{2}\sum_{i=1}^{N}\sigma_i^x\sigma_{i+1}^x \tag{7}$$

$$\hat{H}_1 = -\frac{1}{2}\sum_{i=1}^{N}\sigma_i^z. \tag{8}$$

Here, the undriven Hamiltonian $\hat{H}_0$ consists of nearest-neighbour interactions between N number of spin-$1/2$ particles on a one-dimensional spin network. The transverse field is denoted by $\hat{H}_1$, and is being varied by a time-periodic and harmonic signal $h_z(t) = h_0 + h\cos\omega t$, yielding a time period $T = 2\pi/\omega$ with amplitude h, drive frequency ω, and d.c. field h_0. This Hamiltonian can be readily transformed into a spinless pseudo-fermionic system via the Jordan-Wigner transformation [4]. When written in momentum space spanned by spinors $\psi_k = (c_{-k}, c_k^\dagger)^T$ of fermions at momentum k created (annihilated) by operators $c_k^\dagger$ (c_k), the effective Hamiltonian

$$H(t) = \sum_{(k,-k)-\text{pairs}} \psi_k^\dagger\left[\Big(f_k - h_z(t)\Big)\tau_z + \tau_x\Delta_k\right]\psi_k \tag{9}$$

with $f_k = J\cos k$, $\Delta_k = J\sin k$, τ_{xyz} are the three Pauli Matrices, and the sum is over distinct $(k,-k)$ *Cooper Pairs*. We can transform our system to a frame that rotates with the time-varying symmetry-breaking field. This is achieved by the means of the unitary transformation operator

$$U(t) = \prod_k U_k(t) \tag{10}$$

$$U_k(t) = \exp\left\{\left[\frac{ih}{\omega}\sin\omega t\right]\tau_z\right\}.$$

The resulting transformed Hamiltonian $H'(t) = U^\dagger(t)\ H(t)\ U(t) - iU^\dagger(t)\ \partial_t U(t)$ simplifies to

$$H'(t) = \sum_{(k,-k)-\text{pairs}} \psi_k^\dagger\Big[\tau_z f_k + \tau_x\cos\big(\eta\sin\omega t\big) + \tau_y\sin\big(\eta\sin\omega t\big)\Big]\psi_k, \tag{11}$$

where we defined $\eta = 2h/\omega$. Using the Jacobi-Anger formula [35]

$$e^{i\eta\sin\omega t} = \sum_{n=-\infty}^{\infty} J_n(\eta)\, e^{in\omega t}, \tag{12}$$

where $J_n(\eta)$ are Bessel Functions, the transformed Hamiltonian simplifies to

$$H'(t) = \sum_{\substack{(k,-k)\\ \text{pairs}}} \psi_k^\dagger\Big\{\tau_z f_k + 2\tau_x\Delta_k\sum_{n\geq 0}J_{2n}(\eta)\cos\big(2n\omega t\big) - 2\tau^y\Delta_k\sum_{n\geq 0}J_{2n+1}(\eta)\sin\big[\,(2n+1)\,\omega t\big]\Big\}\psi_k, \tag{13}$$

In the frequency regime $\omega \gg f_k$, the long-time average $H^{RWA} \equiv \lim_{n\to\infty}\frac{1}{nT}\int_0^{nT}\mathrm{d}t\ H'(t)$ can serve as a suitable approximation for $H'(t)$. This approximation, known as the *Rotated Wave Approximation* (RWA), eliminates the oscillating modes and results in an effective Hamiltonian that is independent of time.

$$H^{RWA} = \sum_{(k,-k)-\text{pairs}} \psi_k^\dagger\Big[f_k\tau_z + 2J_0(\eta)\Delta_k\tau_x\Big]\psi_k, \tag{14}$$

It is evident that by manipulating the drive parameters, specifically the amplitude denoted by h and the frequency denoted by ω, in a manner such that η is positioned on a root of $J_0(\eta)$, the fermion number can be conserved to a significant extent at this particular resonance. Consequently, it is feasible to exercise direct control over H^{RWA}, resulting in a comprehensive suppression of the dynamics of otherwise responsive observables.

This phenomenon is highly general in nature, and can be readily adapted to non-integrable systems. In such cases, freezing has the additional effect of inducing DMBL, suppressing thermalization to infinite temperatures. Numerical quantification of localization of a specific (quasi) stationary state in a physically significant representation can be achieved through the computation of the *Inverse Participation Ratio* (IPR). In the position representation, the IPR for a state $|\psi\rangle$ [36–39] is defined as

$$\phi_{IPR} \equiv \int \mathrm{d}\mathbf{x}\ |\ \langle\mathbf{x}|\psi\rangle\ |^4$$

This definition can be generalized to the IPR of a state $|\phi\rangle$ in a representation given by complete orthonormal basis $|m\rangle$ as

$$\phi_{{}_{IPR}} \equiv \sum_m |\ \langle m|\psi\rangle\ |^4. \tag{15}$$

The smallest value of the IPR corresponds to a fully delocalized state, $\psi(x) = 1/\sqrt{N}$ for a system of size N [39, 40]. Values of the IPR close to unity correspond to localized states [41]. For a periodically driven system, we look at the IPR of the quasi-stationary Floquet

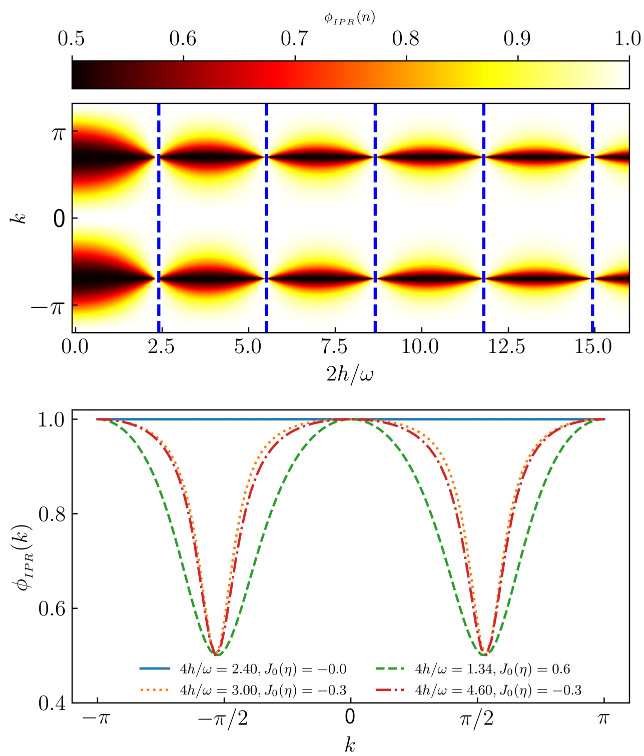

FIG. 1. Reduced IPR (defined in equation 16) for one of the two Floquet modes obtained from the exact dynamics of the TFIM for size $N = 100$ and $\omega = 90$ for the entire Brillouin zone (top panel, ordinate) and a few drive amplitudes (top panel, abscissa). The dashed lines (top panel) indicate the roots of $J_0(\eta)$. The bottom panel shows cross-sections for four different chosen amplitudes.

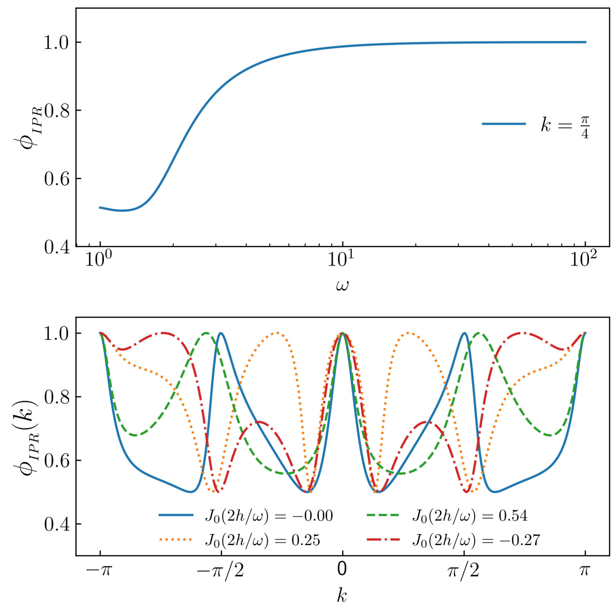

FIG. 2. Reduced IPR obtained by adiabatically increasing ω (top panel abscissa) for one the floquet mode obtained from equation 16 at the root of $J_0(\eta)$ for N = 500. IPR is ~ 0.5 (localized yet not fully freezing) upto $\omega \sim 2$, afterthat, smoothly increased to unity (fully localized and freezibg) at higher $\omega \geq 10$ (top panel, ordiante). At bottom panel cros-sections for four chosen amplitudes at $\omega = 2$ are plotted for a brillouin zone (abscissa) with corresponding reduced IPRs(ordinate).

modes at $t = T$, where $t = 2\pi/\omega$ for drive frequency ω. In the TFIM model, equation 14 indicates that, at resonance, when $J_0(\eta) = 0$, the Floquet modes are approximately given by the fermionic Fock states, which have a trivially unit IPR in the representation of the eigenmodes of the transverse field $\hat{H}_1$ in equation 6. Here, a particular Floquet mode can be decomposed into a direct product of cooper-pair states as $|\phi\rangle = \prod_{k,-k} |\phi_k^n\rangle$. In the RWA limit and at resonance, $|\phi_k^n\rangle$ has values of $|0\rangle, |k, -k\rangle$ for two values of $n = 0, 1$ respectively. We define the reduced IPR of $|\phi_k^n\rangle \; \forall k$ to be

$$\phi_{IPR}^{(n)}(k) = |\langle 0|\phi_k^n\rangle|^4 + |\langle +k, -k|\phi_k^n\rangle|^4, \qquad (16)$$

where $n = 0, 1$. In the RWA limit and at resonance , this quantity is unity, indicating very low participation and the onset of freezing. Figure 1 shows results from numerically simulating the TFIM dynamics. The reduced IPR for a particular Floquet mode recovered by simulating the exact Schrödinger dynamics over a single time period of the drive, and plotted as a function of momentum k for different η's. At resonance, when η lies at the root of the Bessel function $J_0(\eta)$, the IPR is exactly unity for all momenta. Outside this resonance, the IPR is unity only for some momenta because the effective Hamiltonian is perfect diagonal at $k \in \{-\pi, 0, \pi\}$ as can be seen in the cross-sectional plots of figure 1. As we move away from the resonance point, IPR reduces from unity. However, as the TFIM is an integrable spin model, the IPR never drops to a value that is small enough to indicate thermalization. At low frequencies, RWA fails due to the unavailibity of zero off-diagonal terms in the effective transformed Hamiltonian, as well as the absence of integrability breaking terms to counteract the off diagonal terms. Consequently, the IPR remains quite high (~ 0.5) even at the resonance point as can be seen figure 1. At low frequency, this is valid for all momentum and parameter η, see figure 2.

Because the dependence of observable expectations on the eigenstates is always fairly strong for integrable systems like the TFIM, such systems will never exhibit any kind of thermal behaviour unless integrability breaking terms (such as strong disorder) are included [6]. As a result, it is not physically meaningful to refer to the unit IPR region as "*Many Body Localiza-*

tion", because the parameter space lacks a thermalized region to contrast with this state. The type of Floquet Engineering described above, on the other hand, can be easily applied to a broad class of nonintegrable systems where FETH is expected to hold in certain regions. Long-range spin systems, in particular, where the exchange energies between far-off spins are taken into account in the model Hamiltonian, are good candidates because they are known to thermalize when driven with low frequencies [42].

II. LONG RANGE INTERACTIONS: THE LIPKIN MESHKOV GLICK MODEL:

The periodically driven Curie-Weiss model for N long-range spins is described by the Hamiltonian

$$\hat{H}(t) = \hat{H}_0 + \left[h\cos\left(\omega t\right) + h_0\right]\,\hat{H}_1. \tag{17}$$

Here, the undriven part $\hat{H}_0$ and the driven part $\hat{H}_1$ are, respectively,

$$\begin{aligned}\hat{H}_0 &= \frac{1}{2}\sum_{ij} J_{ij}\hat{\sigma}^z_i\hat{\sigma}^z_j, \qquad (18)\\ \hat{H}_1 &= \sum_{i=1}^{N}\hat{\sigma}^x_i.\end{aligned}$$

The Heisenberg exchange energy of the bond between spins i and j is given by

$$J_{ij} = \frac{J_\alpha}{N^{1-\alpha}}\frac{1}{r^\alpha_{ij}}, \tag{19}$$

with r_{ij} representing the smallest graph distance between them. Putting $\alpha = 0$ yields the Lipkin Meshkov Glick (LMG) model with all-to-all interactions $J_{ij} = J_0/N\ \forall(i,j), i\neq j$. We choose to maintain the extensivity of the interaction energy by enforcing the condition

Add refs

$$\frac{J_0}{N}\sum_{i\neq j} 1 = \frac{J_0}{N}\frac{N(N-1)}{2} = 1,$$

yielding the Kac-norm $J_0 = 2/(N-1)$. The Hamiltonian in equation 17 commutes with $P_{ij} \equiv \frac{1}{2}\left(1+\vec{\sigma}_i\cdot\vec{\sigma}_j\right)$. In addition, it also commutes with the total angular momentum $S^2 = \left|\vec{S}\right|^2$, where $\vec{S} = S^x\hat{x} + S^y\hat{y} + S^z\hat{z} \equiv \frac{1}{2}\sum_i\vec{\sigma}_i$. We now choose to populate the system in a state with $S^2 = \frac{N}{2}\left(\frac{N}{2}+1\right)$. In that case, the dynamics remains invariant in the $N+1-$dimensional space spanned by the common eigen states of $P_{ij}, |S|^2$ and S_z; the so-called *Totally Symetric Substace*, or TSS [43]. Let the eigenvalues of S^z in the TSS be s_n, and the eigen vectors be $|s_n\rangle$. Here, $s_n = -\frac{1}{2}+\frac{n}{N}$ and the index $n = 0(1)N$ has $N+1$ values. The dynamics is restricted to this invariant subspace, wherein the matrix elements of the Hamiltonian are given by

$$\begin{aligned}\langle s_i|\hat{H}_0|s_j\rangle &= -\frac{4}{N-1}s_i^2\delta_{ij},\\ \langle s_i|\hat{H}_1|s_j\rangle &= \left[\sqrt{\frac{N}{2}\left(\frac{N}{2}+1\right) - Ns_i(Ns_{i+1})}\,\delta_{i+1,j}\right.\\ &\qquad\left. + \sqrt{\frac{N}{2}(\frac{N}{2}+1) - Ns_i(Ns_{i-1})}\,\delta_{i-1,j}\right]\end{aligned} \tag{20}$$

These allow for a numerical representation of the Hamiltonian in the TSS.

Next, we transform the Hamiltonian to the rotated frame given by the operator

$$\hat{U}(t) = \exp\left[i\frac{h}{\omega}\sin(\omega t)\hat{H}_1\right]. \tag{21}$$

This is analogous to the rotation performed for the TFIM in eqns 10 and 11. Defining $\tau = \frac{h}{\omega}\sin\omega t$, we use the fact that $\hat{H}_1 = 2S^x$, as well as the following identity obtained by using the Baker-Campbell-Hausdorff formula,

$$e^{i2\tau\hat{S^x}}\hat{S^z}e^{-i2\tau\hat{S^x}} = \hat{S^z}\cos\left(2\tau\right) + \hat{S^y}\sin(2\tau), \tag{22}$$

to simplify the transformed Hamiltonian $\tilde{H}(t) = \hat{U}^\dagger(t)\ \hat{H}(t)\ \hat{U}(t) - \hat{U}^\dagger(t)\ \partial_t\hat{U}(t)$, yielding

$$\begin{aligned}\tilde{H}(t) = -\frac{1}{N-1}&\Big[\left(S^z\right)^2\left(1+\cos 4\tau\right) + \left(S^y\right)^2\left(1-\cos 4\tau\right)\\ &+ \left\{S^y, S^z\right\}\sin 4\tau\Big] - 2h_0 S^x.\end{aligned} \tag{23}$$

Next, we define $\eta \equiv 4h/\omega$ and use the Jacobi-Anger formula in eqn 12 to expand $\tilde{H}(t)$. Ignoring constant terms, this yields

$$\tilde{H}(t) \sim \frac{\left(\hat{S}^x\right)^2}{N-1} - 2h_0\hat{S}^x - \frac{J_0(\eta)}{N-1}\left[\left(\hat{S}^z\right)^2 - \left(\hat{S}^y\right)^2\right] - \frac{2}{N-1}\sum_{k=1}^{\infty} J_{2k}(\eta)\,\left[\left(\hat{S}^z\right)^2 - \left(\hat{S}^y\right)^2\right]\,\cos\left(2k\omega t\right)$$
$$- \frac{2}{N-1}\sum_{k=1}^{\infty} J_{2k-1}(\eta)\,\left\{\hat{S}^y, \hat{S}^z\right\}\,\sin\left[(2k-1)\omega t\right]. \tag{24}$$

If ω is large enough to smooth out the harmonic components, we obtain the RWA,

$$\tilde{H}(t) \approx \tilde{H}_{\rm RWA} \equiv \frac{\left(\hat{S}^x\right)^2}{N-1} - 2h_0\hat{S}^x - \frac{J_0(\eta)}{N-1}\left[\left(\hat{S}^z\right)^2 - \left(\hat{S}^y\right)^2\right]. \tag{25}$$

If the drive amplitude h is adjusted such that η lies at a root of $J_0(\eta)$ (the localization point), the RWA Hamiltonian is diagonal in the representation of the transverse field $\hat{S}^x$, yielding an IPR of unity in that representation, similar to the TFIM in the previous section. Note however, that if the DC transverse field h_0 is set to 0, then, at the localization point, the RWA Hamiltonian $\tilde{H}_{\rm RWA} \sim \left(\hat{S}^x\right)^2$. The eigenvalues are two-fold degenerate. This produces infinitely many (Floquet) eigenmodes in the degenerate subspace whose IPRs may not always be unity in the S^x representation. The removal of this degeneracy necessitates the inclusion of the d.c. field h_0. However, note that rational values of h_0 may add accidental degeneracies in $\tilde{H}_{\rm RWA}$. To see this, note that, at a localization point, the eigenvalues of $\tilde{H}_{\rm RWA}$ in the TSS are given by

$$\mathrm{Eigs}\left[\tilde{\mathrm{H}}_{\rm RWA}\right] = \frac{\left(\frac{\mathrm{N}}{2}-\mathrm{m}\right)^2}{\mathrm{N}-1} - 2\mathrm{h}_0\left(\frac{\mathrm{N}}{2}-\mathrm{m}\right), \tag{26}$$

where the half-integer $-N/2 \le m \le N/2$ is the eigenvalue corresponding to a particular eigenstate $|m\rangle$ of the symmetry-breaking field $\hat{S}^x$. In order to ensure that no additional degeneracies occur, we have to set h_0 in such a way that no two energies accidentally coincide. If $N \gg 1$ (substantially large), then this condition can be readily met by assuring that $(1-2h_0)^{-1}$ is never an integer that is divisible by N. To ensure this in our numerical simulations, we have kept h_0 at a small irrational value.

The localization of the Floquet states at resonance is supported by exact numerical results, as can be seen in fig 3. Here, we show plots of the IPR of the Floquet modes $|\phi^n\rangle$ for $S^2 = \left(N/2\right)\left(N/2+1\right)$. The IPR in S^x representation is

$$\phi_{IPR}(n) = \sum_m |\langle m|\phi^n\rangle|^4. \tag{27}$$

These plots were obtained numerically by diagonalizing the propagator $U(t)$ at $t=T$, where $U(t)$ is defined in eqn 5. This propagator was obtained from simulations of the exact quantum dynamics using QuTiP, the Quantum Toolbox in Python [44]. We kept the frequency at a fairly large value $\omega = 90$ where we expect that RWA would be valid, and $N = \mathcal{O}(10^2)$. The density plot in the upper panel of fig 3 depicts the IPR of the Floquet states; the abscissa $\eta = 4h/\omega$ and the ordinate is $n/(2N+1)$, where $n \le 2N$ is a nonnegative integer that indexes the Floquet states in increasing order of

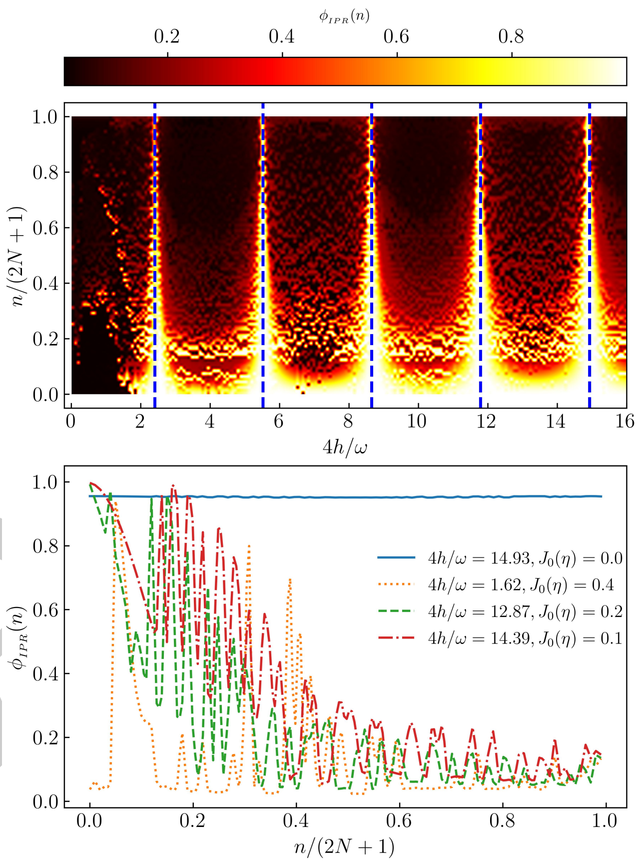

FIG. 3. IPR density plot for all possible Floquet modes (top panel ordinate) for different values of $\eta = 4h/\omega$ (top panel abscissa), deduced from equation 27 for exact LMG Hamiltonian for N = 50. Blue dashed lines are roots of $J_0(\eta)$. At bottom panel cross-section of IPR (ordinate)for four different η's plotted for all possible floquet modes(bottom panel, abscissa) at $\omega = 90$. IPR founds to be $\sim$ unity for all floquet modes at roots of J_0.

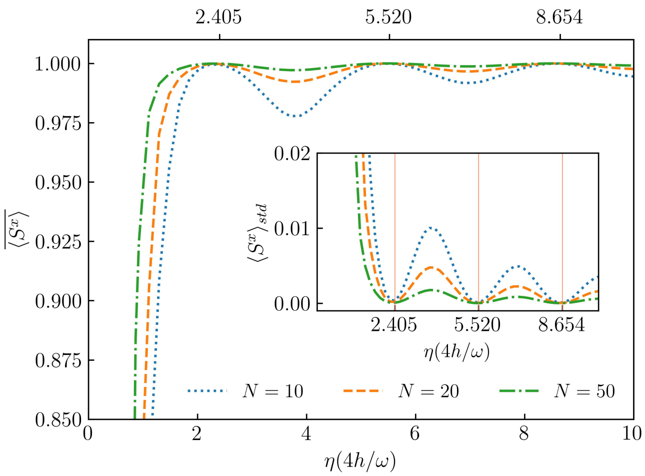

FIG. 4. Temporal average of $\left\langle \hat{S^x} \right\rangle$ (ordinate) for different η's (abscissa) is plotted for $\sim 200T$ at higher ω for different N=10,20,50. $\overline{\langle S^x \rangle}$ is found to be unity at roots of $J_0(\eta)$. At points away from resonance points, $\left\langle \hat{S^x} \right\rangle$ falls below unity. The corresponding standard deviation $\left\langle \hat{S^x} \right\rangle_{std}$ supports the variation of $\overline{\langle S^x \rangle}$ (inset fig.). $\left\langle \hat{S^x} \right\rangle_{std}$ is ~ 0 describing a full freezing of the system at roots of $\mathcal{J}_0(\eta)$ (red vertical solid lines).

m. The dashed vertical lines correspond to the roots of $J_0(\eta)$. Comparing with the IPR of the TFIM in fig 1, we can see a very similar patterns in the immediate neighbourhood of the roots. Evidently, the IPR approaches a value of one for sufficiently large values of the roots, strongly suggesting full DMBL. Deviations occur at the smallest root of $J_0(\eta)$ (around $\eta = 2.405$) due to the contributions from higher order terms in eq 24. Thus, a higher root is favored for DMBL.

The bottom panel of fig 3 contains cross sections of the full IPR plot for selected values of η as indicated in the legend. When the drive amplitude h is adjusted such that η is close to a root of $J_0(\eta)$, the Floquet States are mixed, but not entirely thermal, since the IPR does not fall to $\mathcal{O}(N^{-1})$, indicating that localization persists to some extent. However, the further we are from the roots, the closer the IPR gets to one predicted by thermalization.

Figure 4 shows plots of the long-time average (from $t = 0 - 200T$) of the field amplitude $\left\langle \hat{S^x} \right\rangle$ as a function of η. The system is started from the fully polarized state $s_n = N/2$ in the TSS and the dynamics simulated. The average is plotted for different values of amplitude h, keeping the frequency fixed at a high value of $\omega = 90$. It is clearly very close to unity at roots of $J_0(\eta)$ and falls at points away from it, indicating that S^x is approximately conserved at the localization points.

Small deviations do occur due to the role of higher order terms in the rotated Hamiltonian in eq 23. This can be demonstrated quantitatively by comparing the IPR obtained from the exact dynamics simulation with that obtained from the dynamics of $\tilde{H}(t)$ in eq 23 after truncating the series at orders $k \geq 1$. This comparison can be seen in fig 5. The IPR plots from the exact dynamics indicate that the first localization point, represented by the lowest root of $J_0(\eta)$, does not show complete DMBL. However, DMBL is particularly conspicuous at large roots. The IPRs of the Floquet states obtained from the RWA dynamics exhibit large deviations from unity when away from the localization point as evidenced by the green and red curves in the middle panel of fig 5. However, complete localization is seen in the RWA dynamics at any localization point, in contrast to the exact case in the top panel. Thus, it is necessary to incorporate higher-order corrections into the Rotating Wave Approximation (RWA) at lower localization points. The application of the first-order correction to RWA in the lower panel of fig 5 results in a curve structure that is closer to that from the exact dynamics.

III. PERSISTENCE OF DMBL IN THE CONTINUUM LIMIT

In the continuum limit, where $N \to \infty$, the disparity between neighboring values of s_i in equation 20 can be disregarded, and s_i can be mapped to a continuum $q \in [-1/2, 1/2]$ [43]. We define the Hamiltonian per particle $h(t) \equiv \frac{H(t)}{N}$, and a canonically conjugate coordinate $Np \equiv \left\langle -i\frac{\partial}{\partial q} \right\rangle$. Then, in this limit, the dynamics can be approximated by that of a classical Hamiltonian [45]

$$h(t) = -2q^2 - [h\cos\omega t + h_0]\ \sqrt{1-4q^2}\ \cos p, \tag{28}$$

which yields the dynamical system

$$\begin{aligned} \frac{\mathrm{d}q}{\mathrm{d}t} &= \frac{\partial h}{\partial p} = h(t)\sqrt{1-4q^2}\sin p \\ \frac{\mathrm{d}p}{\mathrm{d}t} &= -\frac{\partial h}{\partial q} = 4q\left[1 - \frac{h(t)\cos p}{\sqrt{1-4q^2}}\right], \end{aligned} \tag{29}$$

where $h(t) = [h\cos\omega t + h_0]$. We have profiled simulations of the ensuing dynamics with the *Poincaré surface of section* (PSOS) of the full dynamics. Here, the (q,p) −phase space is strobed at $t = nT$, and plotted for a large number of initial conditions. The results are shown in the upper panels of fig 6 for a small value of $\omega = 2.5$ (left panel) and a large value $\omega = 90$ (right panel). In both cases, the value of h is chosen such that η lies on the first root of $J_0(\eta)$. The onset of chaos for small drive frequency indicates thermal behaviour

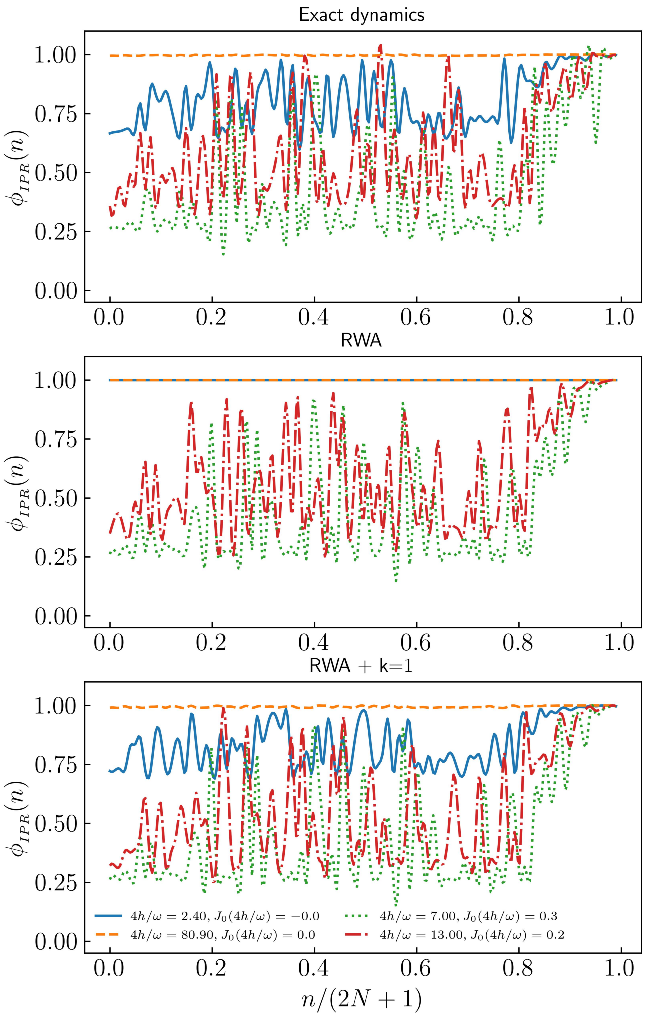

FIG. 5. The comparison between IPR for exact dynamics and RWA with corresponding correction orders. IPR is calculated for four different η's and corresponding $J_0(\eta)$ values for colors, Blue :$\eta = 2.40, J_0(\eta) = 0.0$, dashed orange:$\eta = 80.9, J_0(\eta) = 0.0$, Green:$\eta = 7.0, J_0(\eta) = 0.3$, Red:$\eta = 13, J_0(\eta) = 0.2$. At low root of $J_0(\eta)$ IPR is not unity (Blue curve) where at higher root (orange dashed) it is unity while at points away from roots IPR are less than unity in the exact (top panel) plot. RWA does not matches with the exact plot. At all roots of $J_0(\eta)$ IPR is unity(middle panel). RWA with additional higher order terms exhibit similar system pattern(Bottom panel) with exact dynamics.

for typical initial conditions, with small islands of regularity for others. This is consistent with similar results for small frequencies reported in [42, 46]. *However,* at high frequency, the regular islands distinctly dominate over the chaos. The trajectories indicate that the conservation of $\langle S^x \rangle \approx \sqrt{1-4q^2}\ \cos p$ [43] at high ω persists in the thermodynamic limit. That this is a signature of the underlying quantum dynamics can be readily seen in the quantum phase space representation of the Floquet Eigenstates for a large but finite N. These are shown in the corresponding lower panels of fig 6. Here, we have plotted the Spectral Average of the Husimi Q-functions of the acquired Floquet States in the TSS. Specifically, for a coherent state $|q,p\rangle$, the corresponding Spectral-Averaged Husimi distribution [47] is obtained by

$$H(q,p) \equiv \frac{1}{(2N+1)\pi} \sum_n \langle q,p|\phi^n\rangle \langle \phi^n|q,p\rangle \tag{30}$$

The quantum phase space retains signatures of the classical phase space dynamics when $N = 500$, indicating the onset of the persistence of S^x conservation that arises from the resonance condition at high frequencies.

IV. PHASE CROSSOVER FROM THERMAL TO DMBL

The analysis of the periodically driven LMG model reveals two distinct scenarios at low and high external drive frequencies. In the former case, thermalization in accordance with FETH is seen, whereas in the latter case, DMBL is induced. As a result, we hypothesize that a macroscopic change in phase occurs due to the influence of frequency.

To demonstrate this, we investigate the IPR of the Floquet mode with smallest quasienergy for numerous frequencies and system sizes, along with the associated drive amplitude h keeping the system at a localization point. The results are shown in fig 7 . In the low-frequency range $\omega \in [1.0, 9.0]$, the IPR exhibits values well below unity. Moreover, the IPR gradually diminishes with increasing system size, following a system size inverse proportional trend, which confirms the participation distribution (as shown in the bottom panel). As the limit $N \to \infty$, the inverse participation ratio (IPR) tends towards zero, indicating a fully delocalized state. The plots reveal a gradual increase in the unity of IPR over a certain frequency range, specifically at $\omega \approx 5.0$. In addition, the rise does not cross with those for different values of N, suggesting the onset of a phase crossover [30, 48]. As the size of the system increases, the crossover region becomes smoother, rather than sharper.

We can also look at this crossover more clearly in the plots of the heating rate of the system, defined simply by the expectation value of the Hamiltonian, $\left\langle \hat{H}(t) \right\rangle$. We have carried out the numerical evaluation from the simulated dynamics over $t = 500T$.

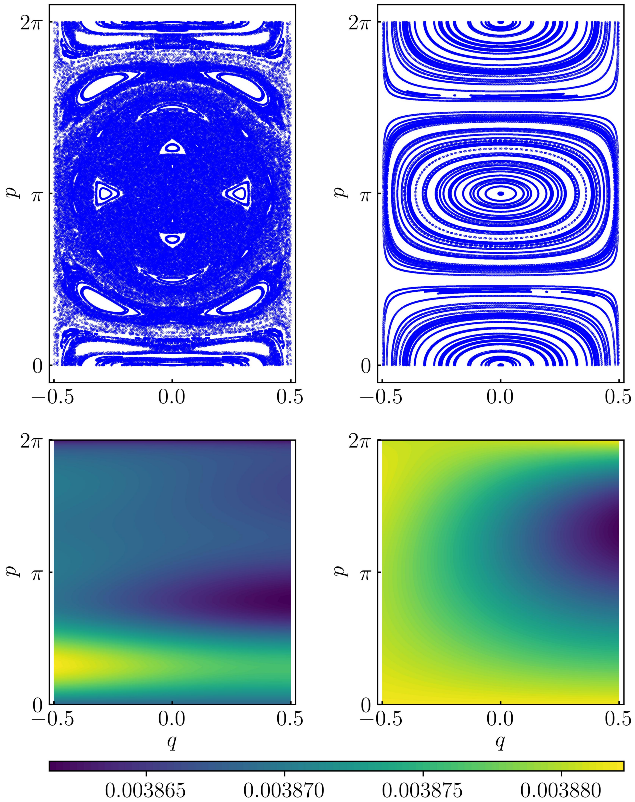

FIG. 6. Phase-space distributions at $\omega = 2.5$ (left panels) and $\omega = 90.0$ (right panels) for 100 initial conditions. At small ω, the classical PSOS, obtained from simulating the dynamics in eqns 29 (top left panel), shows chaotic behaviour, whereas at the higher ω, the onset of regular dynamics can be readily seen (top right panel). The bottom panels plot the corresponding Spectral-Averaged Husimi-Q function, obtained from the Floquet modes $|\phi^n\rangle$ using eqn 30. The $\omega = 2.5-$case (bottom left panel) has a uniform distribution with less contrast in colour. This is consistent with the chaotic behaviour seen in the continuum limit. In the $\omega = 90-$case (bottom right panel), the distribution has distinct colour contrasts, which is consistent with the regular dynamics pattern seen in the continuum limit.

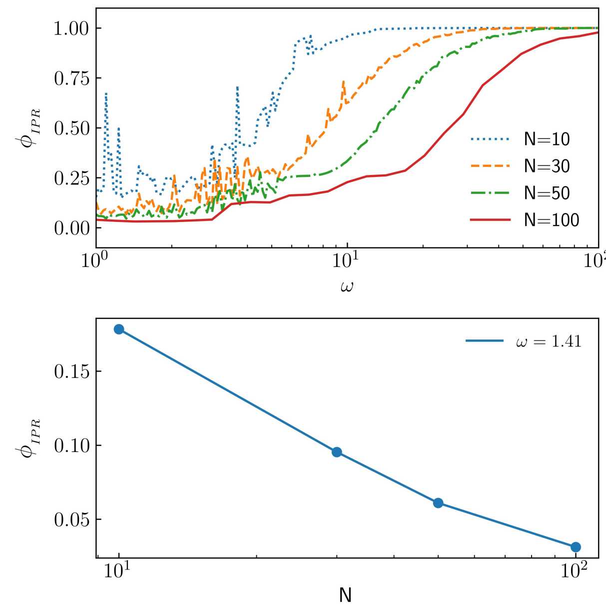

FIG. 7. IPR is plotted (top panel, ordinate) for a range of $\omega \in [1, 100]$(top panel, abscissa) for four different $N = 10, 30, 50, 100$ at root of $J_0(\eta)$. At small ω upto $\omega \sim 10$ IPR founds to be very small and rises slowly upto unity (fully localized) at higher frequencies. At bottom panel IPR (ordinate) is plotted for different $N = 10, 30, 50, 100$(bottom panel, abscissa) for a random small $\omega \sim 1$ at root of $J_0(\eta)$ from the values from top panel. IPR falls as proportianl to inverse of N's value which is a fully distribued state. The smooth rise in IPR defines a phase cross over(top panel) between a fully distributed thermal phase to a fully localized freezing phase.

When the system is adequately described by FETH, the temporal fluctuations in the heating rate, defined by $\langle H\rangle^2_{std} \equiv \overline{\left\langle \hat{H}\right\rangle^2} - \overline{\left\langle \hat{H}\right\rangle}^2$ (see eqn 3), are minimal in the thermodynamic limit, as the spread of states leads to a limited standard deviation[49]. Conversely, the onset of athermality is indicated by nonzero fluctuations in time. If we set the initial state to the fully polarized state in the TSS (given by $|s_N\rangle$), then the onset of freezing, together with DMBL, will result in nearly infinite hysteresis in the ensuing dynamics, causing $|\psi\rangle(t) \approx |s_N\rangle \forall t$. From eqn 17, we can clearly see that this will lead to a linearly rising dependence on ω in $\langle H\rangle_{std}$ as long as we stick to a localization point given by a fixed h/ω. All these observations are corroborated by the heating rate plots in figure 8.

V. CONCLUSION AND OUTLOOK

We have delved into the onset of freezing and phase cross-over in 1D spin systems driven by a time-perodic transverse field, contrasting the responses in the Transverse Field Ising Model (TFIM) with that of the long-range Lipkin-Meshkov-Glick Model (LMG). The parametrization of DMBL is based on the Inverse Participation Ratio (IPR) of the Floquet eigenstates. Our investigations compared the IPRs from both models numerically, and found the emergence of thermal behavior at low frequencies and freezing at high frequencies for the LMG model, the latter a direct consequence of the appearance of additional approximately conserved quantities.

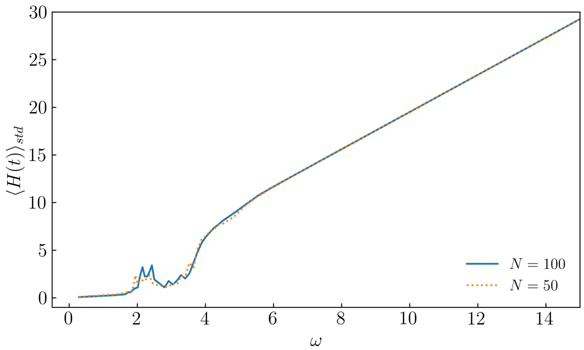

FIG. 8. The standard deviation of the heating rate, denoted by $\langle H\rangle_{std}$, calculated over a span of $t = 500T$ for two system sizes. Here, h is varied to keep $\eta = 4h/\omega$ at the first root of $J_0(\eta)$. A nonsingular rise has been identified at $\omega \approx 4.0$. $\langle H\rangle_{std}$ exhibits a diminutive magnitude below that value of ω, while a linear rise is observed at higher frequencies, consistent with freezing. A vanishingly small standard deviation for $\omega \ll 4.0$ indicates the presence of a thermal region, whereas a larger finite standard deviation suggests the existence of athermal behaviour. The small peaks observed at $\omega \in [2, 4)$ are finite-size effects that disappear in the thermodynamic limit.

A. Conclusion:

Long-range spins exhibit strong localization in spin-coordinate space for the LMG model when the drive frequency is $\omega \gg J$, where J represents the spin exchange energy. The localization of the LMG model occurs at specific resonance points of the drive frequency ω and amplitude h, at $J_0(4h/\omega) = 0,\ \omega \gg J$. This is apparently similar to the phenomenon of Dynamical Freezing (DMF) in the Transverse Field Ising Model (TFIM), where comparable localization at resonance points, determined by the roots of $J_0(2h/\omega)$, occurs due to the onset of an additinal approximate conservation in the transverse field itself. However, a key difference is the thermal behaviour of the LMG model at low frequencies. Plots of the IPR for a range of frequencies along the resonance manifold exhibits a smooth increase in IPR yieling a quantum phase-crossover from a thermal phase governed by the Floquet Eigenstate Thermalization Hypothesis (FETH) to a Dynamically Many-Body localized phase (DMBL). This crossover is absent in the TFIM, as can be readily seen in the significant magnitude of the inverse participation ratio (IPR) even at low frequencies. Thus, the suppression of thermalization through Dynamical Many Body Localization in long-range systems can be controlled via Floquet engineering, even in clean systems without any disorder. Thus, periodically driven long-range spin systems are an excellent tool for investigating disorder-free Many Body Localization, as can be readily seen via the IPR of its Floquet modes.

B. Outlook:

There are several unexplored indicators of DMBL, such as entanglement entropy and level statistics [10], which we defer to future studies. In addition, Halpern in 2019 proposed a quantum engine based on MBL[11] which works between strong localized and thermal phases of the system. In our proposed LMG model, tuning the system parameters by bringing them to the resonance points, then adiabatically cycling the frequency from the thermal region to the DMBL region, can acheive a similar engine without going through a phase transition.

C. Acknowledgements:

One of the authors, MR acknowledges The University of Burdwan for support via a state-funded fellowship. AR acknowledges support from the University Grants Commission (UGC) of India, via BSR Startup Grant No. F.30-425/2018(BSR), as well as from the Science and Engineering Research Board (SERB) Core Research Grant No. CRG/20l8/004002.

[1] S. Bordia Pranjal, Lüschen Henrik, Periodically driving a many-body localized quantum system, Nature Physics **13**, 460 (2017).

[2] S. Sahoo, I. Schneider, and S. Eggert, Periodically driven many-body systems: A floquet density matrix renormalization group study (2019), arXiv:1906.00004 [cond-mat.str-el].

[3] A. Das, Exotic freezing of response in a quantum many-body system, Phys. Rev. B **82**, 172402 (2010).

[4] G. B. Mbeng, A. Russomanno, and G. E. Santoro, The quantum ising chain for beginners (2020), arXiv:2009.09208 [quant-ph].

[5] H. S. Yamada and K. S. Ikeda, Localization and delocalization properties in quasi-periodically-driven one-dimensional disordered systems, Phys. Rev. E **105**, 054201 (2022).

[6] A. Roy and A. Das, Fate of dynamical many-body localization in the presence of disorder, Phys. Rev. B **91**, 121106 (2015).

[7] H. Li, B. Shapiro, and T. Kottos, Floquet scattering theory based on effective hamiltonians of driven systems, Phys. Rev. B **98**, 121101 (2018).

[8] A. Eckardt and E. Anisimovas, High-frequency approximation for periodically driven quantum systems from a floquet-space perspective, New Journal of Physics **17**, 093039 (2015).

[9] L. Zhang, V. Khemani, and D. A. Huse, A floquet model for the many-body localization transition, Phys. Rev. B **94**, 224202 (2016).

[10] V. Khemani, A. Lazarides, R. Moessner, and S. L. Sondhi, Phase structure of driven quantum systems, Phys. Rev. Lett. **116**, 250401 (2016).

[11] N. Yunger Halpern, C. D. White, S. Gopalakrishnan, and G. Refael, Quantum engine based on many-body localization, Phys. Rev. B **99**, 024203 (2019).

[12] S. Aditya and D. Sen, Dynamical localization and slow thermalization in a class of disorder-free periodically driven one-dimensional interacting systems (2023), arXiv:2305.06056 [cond-mat.stat-mech].

[13] Z. Papić, E. M. Stoudenmire, and D. A. Abanin, Many-body localization in disorder-free systems: The importance of finite-size constraints, Annals of Physics **362**, 714 (2015).

[14] T. Nag, S. Roy, A. Dutta, and D. Sen, Dynamical localization in a chain of hard core bosons under periodic driving, Phys. Rev. B **89**, 165425 (2014).

[15] A. Campa, T. Dauxois, and S. Ruffo, Statistical mechanics and dynamics of solvable models with long-range interactions, Physics Reports **480**, 57 (2009).

[16] E. R. S. Eisele, Theodor, Multiple phase transitions in the generalized curie-weiss model, Journal of Statistical Physics , 161 (1988).

[17] A. Canning, A class of long range ising spin models described by curie-weiss mean field theory, Physica A: Statistical Mechanics and its Applications **185**, 254 (1992).

[18] D. Vu, K. Huang, X. Li, and S. Das Sarma, Fermionic many-body localization for random and quasiperiodic systems in the presence of short- and long-range interactions, Phys. Rev. Lett. **128**, 146601 (2022).

[19] G. Misguich, V. Pasquier, and J.-M. Luck, Inverse participation ratios in the xxz spin chain, Phys. Rev. B **94**, 155110 (2016).

[20] M. Calixto and E. Romera, Inverse participation ratio and localization in topological insulator phase transitions, Journal of Statistical Mechanics: Theory and Experiment **2015**, P06029 (2015).

[21] K. Fujii, Introduction to the rotating wave approximation (rwa): Two coherent oscillations, Journal of Modern Physics **8**, 2042 (2017).

[22] D. A. Abanin, E. Altman, I. Bloch, and M. Serbyn, Colloquium: Many-body localization, thermalization, and entanglement, Rev. Mod. Phys. **91**, 021001 (2019).

[23] M. Srednicki, Chaos and quantum thermalization, Phys. Rev. E **50**, 888 (1994).

[24] M. Srednicki, The approach to thermal equilibrium in quantized chaotic systems, Journal of Physics A: Mathematical and General **32**, 1163 (1999).

[25] M. Holthaus, Floquet engineering with quasienergy bands of periodically driven optical lattices, Journal of Physics B: Atomic, Molecular and Optical Physics **49**, 013001 (2015).

[26] M. Vogl, M. Rodriguez-Vega, and G. A. Fiete, Effective floquet hamiltonian in the low-frequency regime, Phys. Rev. B **101**, 024303 (2020).

[27] M. Bukov, L. D'Alessio, and A. Polkovnikov, Universal high-frequency behavior of periodically driven systems: from dynamical stabilization to floquet engineering, Advances in Physics **64**, 139 (2015).

[28] L. D'Alessio and M. Rigol, Long-time behavior of isolated periodically driven interacting lattice systems, Phys. Rev. X **4**, 041048 (2014).

[29] R. Yousefjani, S. Bose, and A. Bayat, Floquet-induced localization in long-range many-body systems, Phys. Rev. Res. **5**, 013094 (2023).

[30] P. Sierant, M. Lewenstein, A. Scardicchio, and J. Zakrzewski, Stability of many-body localization in floquet systems, Phys. Rev. B **107**, 115132 (2023).

[31] R. Yousefjani, S. Bose, and A. Bayat, Floquet-induced localization in long-range many-body systems, Phys. Rev. Res. **5**, 013094 (2023).

[32] F. Alet and N. Laflorencie, Many-body localization: An introduction and selected topics, Comptes Rendus Physique **19**, 498 (2018).

[33] S. J. Garratt and S. Roy, Resonant energy scales and local observables in the many-body localized phase, Phys. Rev. B **106**, 054309 (2022).

[34] R. B. Stinchcombe, Ising model in a transverse field. i. basic theory, Journal of Physics C: Solid State Physics **6**, 2459 (1973).

[35] F. E. H. George Arfken, Hans Weber, *Mathematical Methods for Physicists*, 7th ed. (Academic Press).

[36] S. Mukherjee, A. Spracklen, D. Choudhury, N. Goldman, P. Öhberg, E. Andersson, and R. R. Thomson, Modulation-assisted tunneling in laser-fabricated photonic wannier–stark ladders, New Journal of Physics **17**, 115002 (2015).

[37] S.-H. Lin, B. Sbierski, F. Dorfner, C. Karrasch, and F. Heidrich-Meisner, Many-body localization of spinless fermions with attractive interactions in one dimension, SciPost Phys. **4**, 002 (2018).

[38] N. C. Murphy, R. Wortis, and W. A. Atkinson, Generalized inverse participation ratio as a possible measure of localization for interacting systems, Phys. Rev. B **83**, 184206 (2011).

[39] E. J. Torres-Herrera, I. Vallejo-Fabila, A. J. Martínez-Mendoza, and L. F. Santos, Self-averaging in many-body quantum systems out of equilibrium: Time dependence of distributions, Phys. Rev. E **102**, 062126 (2020).

[40] N. Trivedi and D. Heidarian, Can disorder drive a mott insulator into a metal in 2d?, Progress of Theoretical Physics Supplement **160**, 296 (2005).

[41] G. Misguich, V. Pasquier, and J.-M. Luck, Inverse participation ratios in the xxz spin chain, Phys. Rev. B **94**, 155110 (2016).

[42] A. Russomanno, R. Fazio, and G. E. Santoro, Thermalization in a periodically driven fully connected quantum ising ferromagnet, Europhysics Letters **110**, 37005 (2015).

[43] T. Mori, Prethermalization in the transverse-field ising chain with long-range interactions, Journal of Physics A: Mathematical and Theoretical **52**, 054001 (2019).

[44] J. Johansson, P. Nation, and F. Nori, Qutip 2: A python framework for the dynamics of open quantum systems, Computer Physics Communications **184**, 1234.

[45] B. Sciolla and G. Biroli, Quantum quenches and off-equilibrium dynamical transition in the infinite-dimensional bose-hubbard model, Phys. Rev. Lett. **105**, 220401 (2010).

[46] R. A. Kidd, M. K. Olsen, and J. F. Corney, Quantum chaos in a bose-hubbard dimer with modulated tunneling, Phys. Rev. A **100**, 013625 (2019).

[47] A. Bäcker, S. Fürstberger, and R. Schubert, Poincaré husimi representation of eigenstates in quantum billiards, Phys. Rev. E **70**, 036204 (2004).

[48] S. Sachdev, *Quantum Phase Transitions*, 2nd ed. (Cambridge University Press, Cambridge, 2011).

[49] P. Reimann, Symmetry-prohibited thermalization after a quantum quench, Journal of Statistical Mechanics: Theory and Experiment **2021**, 103106 (2021).

[50] L. Reichl, *The Transition to Chaos: Conservative Classical and Quantum Systems*, Fundamental Theories of Physics, Vol. 200 (Springer International Publishing).

[51] N. Srivatsa, R. Moessner, and A. E. Nielsen, Many-body delocalization via emergent symmetry, Phys. Rev. Lett. **125**, 240401.

[52] Quantum ising phase transition.

[53] B. Marcos, A. Gabrielli, and M. Joyce, Relaxation of quasi-stationary states in long range interacting systems and a classification of the range of pair interactions, Open Physics **10**, 676.

[54] A. Haldar and A. Das, Dynamical many-body localization and delocalization in periodically driven closed quantum systems, Annalen der Physik **529**, 1600333.

[55] J. M. Deutsch, Quantum statistical mechanics in a closed system, Phys. Rev. A **43**, 2046 ().

[56] E. W. Hobson, On the Second Mean-Value Theorem of the Integral Calculus (1909).

[57] M. Rigol and M. Srednicki, Alternatives to eigenstate thermalization, Physical Review Letters **108**, 10.1103/physrevlett.108.110601 (2012).

[58] J. M. Deutsch, Eigenstate thermalization hypothesis, IOP Publishing Ltd **81**, 296 ().

[59] R. Nandkishore and D. A. Huse, Many-body localization and thermalization in quantum statistical mechanics, Annual Review of Condensed Matter Physics **6**, 15 (2015), https://doi.org/10.1146/annurev-conmatphys-031214-014726.

[60] L. D'Alessio and A. Polkovnikov, Many-body energy localization transition in periodically driven systems, **333**, 19.

[61] S. Notarnicola, F. Iemini, D. Rossini, R. Fazio, A. Silva, and A. Russomanno, From localization to anomalous diffusion in the dynamics of coupled kicked rotors, Phys. Rev. E **97**, 022202 (2018).

[62] A. Lazarides, A. Das, and R. Moessner, Fate of many-body localization under periodic driving, Phys. Rev. Lett. **115**, 030402 (2015).